



HAL
open science

Mixing in weakly turbulent stably stratified flows

Chantal Staquet, Pascale Bouruet-Aubertot

► **To cite this version:**

Chantal Staquet, Pascale Bouruet-Aubertot. Mixing in weakly turbulent stably stratified flows. Dynamics of Atmospheres and Oceans, 2001, 34, pp.81-102. 10.1016/S0377-0265(01)00062-8. hal-00264603

HAL Id: hal-00264603

<https://hal.science/hal-00264603>

Submitted on 30 Jan 2023

HAL is a multi-disciplinary open access archive for the deposit and dissemination of scientific research documents, whether they are published or not. The documents may come from teaching and research institutions in France or abroad, or from public or private research centers.

L'archive ouverte pluridisciplinaire **HAL**, est destinée au dépôt et à la diffusion de documents scientifiques de niveau recherche, publiés ou non, émanant des établissements d'enseignement et de recherche français ou étrangers, des laboratoires publics ou privés.



Distributed under a Creative Commons Attribution - NonCommercial 4.0 International License

Mixing in weakly turbulent stably stratified flows

C. Staquet^{a,*}, P. Bouruet-Aubertot^b

^a *LEGI, B.P. 53, 38041 Grenoble Cedex 9, France*

^b *LODYC, Université Pierre et Marie Curie, 4 Place Jussieu, Boîte 100, 75252 Paris Cedex 05, France*

We analyse mixing in three weakly turbulent stably stratified flows, namely low amplitude breaking internal gravity waves, stably stratified homogeneous decaying turbulence and a stably stratified unstable shear layer. We use the method proposed by Winter et al. [J. Fluid Mech. 289 (1995) 115], which provides an exact expression of the diffusive flux of density responsible for mixing. When the three flows have stabilized and organized into quasi-horizontal layers, we show that the diffusion coefficient behaves linearly as a function of a dynamical parameter that characterizes the largest scales of the flow (a Froude number squared or the inverse of a Richardson number) and we provide a simple expression of this linear law.

Keywords: Stably stratified flows; Turbulence; Mixing

1. Introduction

In a stably stratified inviscid fluid, the restoring action of the buoyancy force prevents vertical transport of mass from occurring: any fluid particle displaced vertically from its equilibrium position will oscillate around this position so that the net vertical displacement of the particle over a phase period will be zero. It follows that vertical transport of mass in a stably stratified fluid can only result from molecular diffusion, that is, from mixing. This does not mean that the vertical diffusivity of density is equal to the molecular diffusivity at all times: turbulent motions put into contact fluid particles with each other so that diffusive exchange of mass (which is roughly proportional to the density difference between the fluid particles) will be promoted. Fluid mixing is therefore enhanced, if the diffusive time scale of the motions which advect the fluid particles is not too large compared to the advective time scale.

The purpose of this note is to show that weakly turbulent stably stratified flows, in which the dissipation rate of kinetic energy is controlled by horizontal motions with a vertical shear,

* Corresponding author. Fax: +33-4-76-82-52-71.
E-mail address: chantal.staquet@hmg.inpg.fr (C. Staquet).

share a common feature when their mixing properties are compared. We focus upon three different flows, namely low amplitude breaking internal gravity waves, a three-dimensional homogeneous stably-stratified turbulence and a stably stratified shear layer, in two and three dimensions. The Boussinesq equations are solved for this purpose, using direct numerical simulations. Mixing is analysed using the method derived by Winters et al. (1995) and Winters and D’Asaro (1996), which allows one to compute exactly the diffusive flux of density resulting in fluid mixing. This flux occurs across surfaces of constant density (rather than vertically) and is referred to as the diapycnal flux.

We shall show that in the three flows we consider, the diapycnal diffusivity displays the same dependency as a function of a dynamical parameter that characterizes the largest scales of the flow and we provide a simple expression of this law. The dynamical parameter is a Froude number when there is no background shear and a Richardson number when there is a mean shear.

The outline of the paper is the following. In Section 2, the method of mixing analysis is described, along with the numerical method we use to solve the equations of motions. Sections 3–5 successively report about the three flows we consider: in each section, we briefly specify the equations of motion that drive the flow dynamics, provide the striking features of those dynamics and focus upon the common mixing law shared by the three flows. Conclusions are drawn in Section 6.

A subset of the results presented in Sections 4 and 5 can be found in Godeferd and Staquet (2001) and Staquet (2000), respectively, while Section 3 complements results obtained by Bouruet-Aubertot et al. (2001). The purpose of the present paper, in gathering these results and in further analysing them within a common frame, is to suggest that a characteristic law may exist between mixing and the large scale dynamics in weakly turbulent stably stratified flows.

2. Methodology

2.1. Analysis of mixing

The quantification of mixing in a stably stratified fluid relies upon the estimate of a mixing rate, which is the rate of increase per time unit of potential energy resulting from fluid mixing. This potential energy is denoted E_b in the following. It is only a part of the total potential energy of the flow, E_p , and was characterized by Lorenz (1955) as being its instantaneous minimum value: E_b is the potential energy of the fluid when all motions have ceased and the fluid has returned to rest. Lombard et al. (1990) showed that E_b is the potential energy of a stable density profile introduced by Thorpe (1977), obtained by sorting adiabatically the fluid particles so that the heaviest fluid particle has the lowest altitude. This sorted profile, which we shall refer to as $\rho_b(z)$, is stable by construction. The third step, realized by Lombard et al. (1990), was to compute the rate of change of E_b (i.e. \dot{E}_b) from the sorted profile. This problem was solved by Winters et al. (1995) who provided analytical expressions for the fluxes that control \dot{E}_b . These fluxes are the diapycnal flux, denoted Φ_d , as well as, if mass flux occurs across the bounding surface of the fluid domain, advective and diffusive mass fluxes across that surface. The latter fluxes are denoted $\dot{E}_b^{\text{surf adv}}$ and

$\dot{E}_b^{\text{surf dif}}$, respectively. The temporal evolution of E_b thus obeys the equation

$$\dot{E}_b = \Phi_d + \dot{E}_b^{\text{surf adv}} + \dot{E}_b^{\text{surf dif}}. \quad (1)$$

Among the three flows we consider, the surface fluxes are zero for the shear layer only.

A local diapycnal flux $\phi_d(z, t)$ may also be defined, whose volume average is equal to Φ_d/g , g being the modulus of the acceleration of gravity \vec{g} . $\phi_d(z, t)$ is expressed as (Winters and D'Asaro, 1996)

$$\phi_d(z, t) = -\kappa \frac{\langle |\nabla \rho|^2 \rangle_I}{d\rho_b/dz}, \quad (2)$$

where the average $\langle \cdot \rangle_I$ is performed on an isopycnal surface; z denotes the vertical coordinate and κ the molecular diffusivity of density.

When the fluid has returned to rest (if there is no shear) or to a hydrostatic balanced laminar state (if there is a horizontal mean shear), the diffusive flux of density results from purely molecular effects. We shall refer to this flux as Φ_i . Its expression is

$$\Phi_i = \kappa g \frac{\Delta \rho}{H}, \quad (3)$$

where $\Delta \rho$ is the density difference across the fluid domain and H is the domain height. $\Phi_d - \Phi_i$ is therefore the *fluctuating* diapycnal flux. Φ_i is the minimum value of Φ_d so that $\Phi_d - \Phi_i$ is always positive.

Since the background potential energy E_b results from the irreversible process of mixing, $E_p - E_b$ defines the potential energy associated with reversible processes. The latter energy is usually referred to as the available potential energy and denoted E_a . It is the potential energy of the density fluctuations about the sorted density profile. From the equation for the total potential energy

$$\dot{E}_p = \Phi_a + \Phi_i + \dot{E}_p^{\text{surf adv}} + \dot{E}_p^{\text{surf dif}}, \quad (4)$$

and from Eq. (1), one infers immediately the equation that governs the rate of change of E_a

$$\dot{E}_a = \Phi_a - (\Phi_d - \Phi_i) + (\dot{E}_p^{\text{surf adv}} - \dot{E}_b^{\text{surf adv}}) + (\dot{E}_p^{\text{surf dif}} - \dot{E}_b^{\text{surf dif}}), \quad (5)$$

where Φ_a is the vertical advective flux of density; the last two terms in Eqs. (4) and (5) account for the rate of change of E_p and E_a , respectively, due to advective and surface mass fluxes across the bounding surface of the fluid domain. Eq. (5) shows that, in the fluid interior, a part of E_a is reversibly converted into vertical kinetic energy, at a rate equal to Φ_a while another part is irreversibly converted into fluctuating background potential energy, at a rate equal to $\Phi_d - \Phi_i$ (Winters et al., 1995).

Several estimators of mixing have been proposed in the literature (see, for instance Fernando, 1991) and we shall focus in the present paper upon two of them. These are the diapycnal diffusivity and the mixing efficiency, which we now define.

As any diffusion coefficient, the diapycnal diffusivity K_ρ is defined by the ratio of the flux of scalar along the background scalar gradient (ϕ_d) divided by this scalar gradient

$(-d\rho_b/dz)$. Hence (Winters and D'Asaro, 1996)

$$K_\rho = \frac{\phi_d}{-d\rho_b/dz}. \quad (6)$$

The efficiency of mixing (within the interior of the fluid domain) accounts for the amount of energy gained per time unit through the mixing process, Φ_d , relative to the amount of energy brought to the fluid per time unit, \dot{M} say. When the fluid system is not forced, which is the case in the three flows we consider, the dissipation rate of kinetic energy ϵ is used in place of \dot{M} . Also, only mixing resulting from the flow dynamics, that is from density fluctuations about the sorted density profile, are of interest so that the fluctuating diapycnal flux $\Phi_d - \Phi_i$ should be employed in place of Φ_d . The definition of the mixing efficiency we shall use is thus

$$\gamma = \frac{\Phi_d - \Phi_i}{\epsilon}. \quad (7)$$

2.2. Mathematical model and numerical method

The dynamics of the flows we consider are driven by the Navier–Stokes equations in the Boussinesq approximation: density fluctuations about a hydrostatic balanced state are supposed to be small enough (in magnitude and frequency) for the fluid motions to be incompressible. The effect of these density fluctuations upon the fluid motions comes into play through a buoyancy force (difference between the gravity and the Archimedean forces). These equations display a different form for each flow we consider so that their expression will be written in the next sections. The boundary conditions are either periodic or of the free slip type along the horizontal boundaries.

The Boussinesq equations are solved by a classical pseudo-spectral method (e.g. Canuto et al., 1988): the spatial derivatives are computed using Fourier transforms while the nonlinear terms are computed in physical space. The latter computation produces aliasing errors, which are eliminated in Fourier space by a standard truncation procedure. Time is advanced using a third order Adams–Bashforth scheme. When the boundary conditions are of the free slip type along a boundary, the numerical domain is doubled about that boundary assuming symmetry or antisymmetry properties of the fields about it. These fields become periodic upon the doubled domain and can be expanded in Fourier series. The specific properties of the associated Fourier coefficients are used to reduce the computation time, following a now classical method proposed by Orszag (1971).

The analysis of mixing described in the previous section relies upon a sorted density profile, whose computation is performed as follows. The value of the density field at each grid point is identified with one fluid particle. These fluid particles are next sorted out with their density. The sorted density profile is constructed by filling out each horizontal plane with the heaviest fluid particles, starting with the bottom plane of the numerical domain. Because the density slightly varies from particle to particle, it is averaged over each plane to yield a one-dimensional profile. The word *plane* should be replaced by *line* when the flow evolves in two dimensions.

3. Breaking internal gravity waves of low amplitude

3.1. Overall flow dynamics

We consider a stably stratified fluid in which the Brunt–Väisälä frequency

$$N = \left(-\frac{g}{\rho_0} \frac{d\rho_{\text{lin}}}{dz} \right)^{1/2} \quad (8)$$

has a constant value. $\rho_0 + \rho_{\text{lin}}$ is the density of a hydrostatic balanced state, ρ_0 being a constant reference density and $\rho_{\text{lin}}(z)$ a linear density profile. A monochromatic, high frequency (that is close to N) internal gravity wave of low amplitude, hereafter referred to as the primary wave, propagates in this fluid. Low amplitude means that the isopycnals are only slightly tilted with respect to the horizontal and far from overturning. We have studied the dynamics of this wave in the vertical plane formed by \vec{g} and its wave vector \vec{k} . The restriction to two-dimensional dynamics is motivated by a linear stability analysis by Klostermeyer (1991), which predicts that such a low amplitude wave is most unstable to two-dimensional perturbations in the (\vec{g}, \vec{k}) plane. Comparison of the two-dimensional wave dynamics with a three-dimensional computation (Bouruet-Aubertot et al., 2001) and with laboratory experiments (Benielli and Sommeria, 1996) confirms the validity of the two-dimensional approach when flow statistics are compared.

Let us consider a coordinate system $(0, x, y, z)$, where (x, z) is the vertical plane of the primary wave with z pointing upwards. The Boussinesq equations in this plane are

$$\frac{\partial \nabla^2 \psi}{\partial t} + \mathcal{J}(\nabla^2 \psi, \psi) = \frac{\partial \rho'}{\partial x} + \nu (\nabla^2)^2 \psi \quad (9)$$

$$\frac{\partial \rho'}{\partial t} + \mathcal{J}(\rho', \psi) = -N^2 \frac{\partial \psi}{\partial x} + \frac{\nu}{Pr} \nabla^2 \rho'. \quad (10)$$

As is customary, the use of a stream function ψ such that $u = -\partial\psi/\partial z$ and $w = \partial\psi/\partial x$ implies that the incompressibility condition is satisfied implicitly. $\rho'(x, z, t)$ is the density fluctuation about the hydrostatic density profile mentioned above, scaled as an acceleration: $\rho'(x, z, t) = (g/\rho_0)(\rho(x, z, t) - (\rho_0 + \rho_{\text{lin}}(z)))$, where $\rho(x, z, t)$ denotes the total density. \mathcal{J} is the nonlinear Jacobian operator, ν the kinematic viscosity and

$$Pr = \frac{\nu}{\kappa} \quad (11)$$

is the Prandtl number of the fluid (κ has been defined in the previous section).

The fluid domain is a square box and periodic boundary conditions are used along the two directions. Eqs. (9) and (10) are initialized with a propagating internal gravity wave (the primary wave) of wave vector $\vec{k} = (1, 0, 1)$, Froude number $A(|\vec{k}|/2\pi)^2/N$ equal to 0.013 and Reynolds number $Re = A/\nu$ equal to 10700. A is the initial amplitude of the stream function of the wave and N is set to 1. Four computations will be presented in this section, with resolution 512^2 , which differ only in the value of the Prandtl number: $Pr = 0.72, 1, 5$ and 10 .

Whether propagating (Koudella and Staquet, 2001) or standing (Bouruet-Aubertot et al., 1995), the dynamics of the wave display the same behaviour: it becomes unstable through

parametric instability among resonant triads, a result predicted theoretically by Drazin (1977) and Mied (1976) for a propagating wave. The damping action of viscosity at small scales selects a range of unstable triads, among which the numerical grid operates a second selection. One particular triad eventually grows, which controls the whole instability. The amplification of the resonant waves within the triad, through extraction of energy from the primary wave, eventually makes the latter wave break. Breaking means here that the primary wave loses its coherence (but it does not grow in amplitude). A turbulent regime sets in, where the kinetic energy and potential energy spectra display a k_z^{-3} law, k_z being the vertical wavenumber. This regime lasts a few Brunt–Väisälä periods ($2\pi/N$) only because the primary wave is not forced (see Bouruet-Aubertot et al., 1996 for standing waves; Koudella, 1999 for propagating waves). The breaking of the wave is illustrated in Fig. 1 for a propagating primary wave.

3.2. Analysis of mixing

Wavebreaking in an unforced uniformly stably stratified fluid appears to result in weak fluid mixing over the duration the (laboratory or numerical) experiments are conducted (e.g. McEwan, 1983; Taylor, 1992; Benielli and Sommeria, 1996; Bouruet-Aubertot et al., 2001). The reason is that the energy input to the fluid, a part of which only will be available for mixing, is much smaller than the potential energy of the background density profile. This point may be expressed alternately by noting that the vertical scale of the wave instability is much smaller than that of the background density profile. In laboratory experiments of an internal gravity wave propagating along an interface by contrast, the breaking of the wave may destroy the interface when the wave amplitude becomes comparable to the thickness of that interface (e.g. Hannoun and List, 1988). It follows that, when unforced wavebreaking occurs in a linearly stratified fluid, the sorted density profile only slightly departs from the linear profile: relative changes are smaller than 1% and are associated with modulations of $d\rho_b/dz$ over thin layers, whose thickness has been estimated in Bouruet-Aubertot et al. (2001). These changes, which would initiate the formation of density steps if the wave were forced, are ignored in the following. We shall thus consider that $\rho_b(z, t) \simeq \rho_{\text{lin}}(z)$ (this approximation being further discussed at the end of this section). The diapycnal diffusivity (6) therefore takes the simpler expression

$$K_\rho(z, t) \simeq \frac{g}{\rho_0} \frac{\phi_d(z, t)}{N^2}. \quad (12)$$

We shall focus in this section upon the relation between the diapycnal diffusivity (averaged over the height of the fluid domain) and a Froude number associated with the largest scales of the flow. The Froude number we consider is defined as follows:

$$Fr_t = \frac{\sqrt{2Z}}{N} = \left(\frac{\epsilon}{\mu N^2} \right)^{1/2}, \quad (13)$$

where Z is half the domain averaged vorticity squared and $\epsilon = 2\mu Z$ denotes the dissipation rate of kinetic energy per unit area ($\mu = \rho_0\nu$ is the dynamical viscosity). In ordinary turbulence, such a Froude number is associated with the smallest scales of the flow

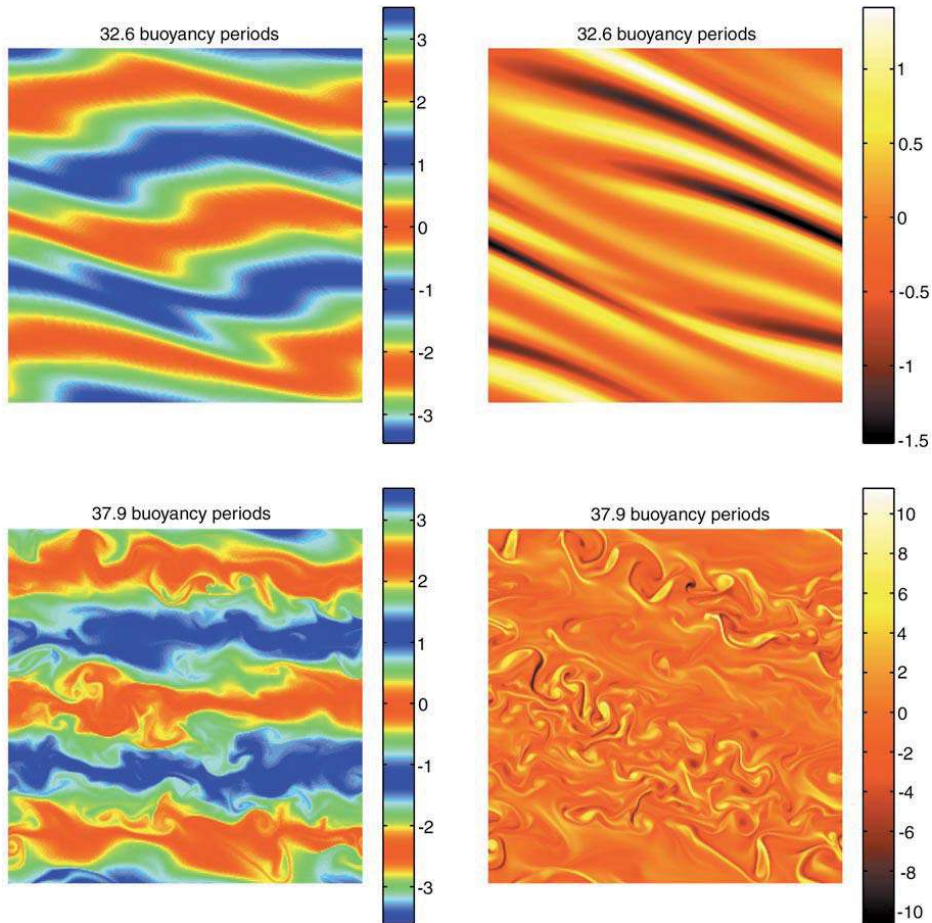


Fig. 1. Contours of the density field (left column) and vorticity field (right column) in the (x, z) vertical plane, for an internal gravity wave of Froude number $Fr_\Gamma = 0.013$ and Prandtl number $Pr = 1$ propagating toward the upper right corner of the domain. *Upper row*: views at $Nt/2\pi = 32.6$, shortly before breaking occurs: the parametric instability that grows through resonant interaction with the primary wave is of large enough amplitude to be visible. It is manifested as vorticity bands of alternate sign, organized into a wave packet (right frame). *Lower row*: the fields are displayed one Brunt–Väisälä period later, just after breaking has occurred. The vorticity layers have become unstable (the origin of this instability is discussed in Koudella and Staquet (2001)).

(e.g. Imberger and Boashash, 1986). In the present case where the kinetic energy spectrum evolves as k_z^{-3} , however, the enstrophy spectrum evolves as k_z^{-1} , meaning that the volume averaged enstrophy is controlled by the largest scales of the flow. Hence, in stably stratified turbulence resulting from internal gravity wave breaking, Fr_Γ is a dynamical parameter associated with the largest scales.

This turbulent regime is statistically homogeneous along the vertical direction so that the diapycnal diffusivity K_ρ may be averaged along the vertical direction. Normalizing this averaged value by the molecular diffusivity κ yields an estimate of the Cox number

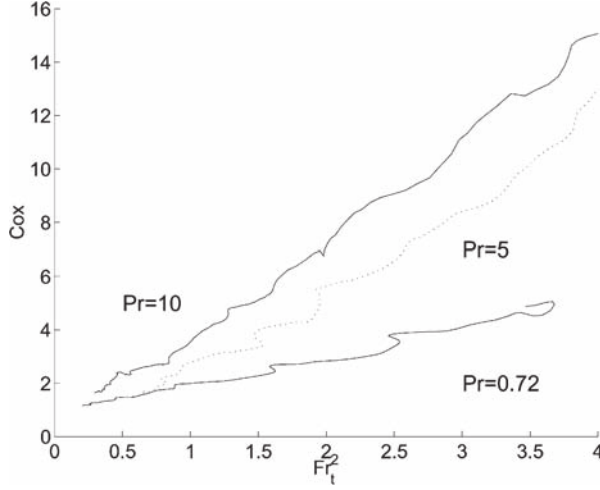


Fig. 2. Instantaneous Cox number $Cox(t)$ defined by Eq. (14) as a function of the Froude number squared $Fr_t^2(t)$ defined by Eq. (13) for the runs with $Pr = 0.72$ (—, bottom curve), $Pr = 5$ (···), $Pr = 10$ (—, top curve). All times after breaking are shown ($Nt/2\pi \geq 35$).

(Osborn and Cox, 1972)

$$Cox \equiv \frac{1}{H} \int_0^H \frac{K_\rho}{\kappa} dz = \frac{\Phi_d}{\Phi_i}, \quad (14)$$

where Φ_i has the simple expression $\kappa\rho_0N^2$ in the present case of a uniformly stably stratified fluid and H is the domain height, as before.

The instantaneous values of the Cox number and of the turbulent Froude number have been computed at all times of the runs having $Pr = 0.72, 5$ and 10 . $Cox(t)$ is plotted as a function of $Fr_t^2(t)$ in Fig. 2, once breaking has occurred. A linear law is displayed for the smallest values of Fr_t^2 , which can be modelled by the following simple expression. From definition (7) for γ , one has: $\Phi_d = \epsilon\gamma + \Phi_i$. Expressing ϵ as a function of the turbulent Froude number (13), we find $\Phi_d = \gamma\mu N^2 Fr_t^2 + \Phi_i$. Dividing by Φ_i yields

$$Cox = \gamma Pr Fr_t^2 + 1, \quad (15)$$

where Pr is the Prandtl number. The coefficient of the linear law inferred from Fig. 2 is thus γPr . It yields a value for γ equal to $\simeq 1.2$ for $Pr = 0.72$, $\simeq 0.5$ for $Pr = 5$ and $\simeq 0.35$ for $Pr = 10$.

The validity of expression (15) to account for the linear law displayed in Fig. 2 relies upon the mixing efficiency to have reached a constant value once breaking has occurred. γ is plotted as a function of time in Fig. 3: it seems indeed to relax toward an asymptotic value after breaking, with the approach faster as the Prandtl number increases. The estimated asymptotic values are lower than those inferred from Fig. 2 using the law (15) and an argument to account for this behavior is provided in the last paragraph of this section.

The existence of final steady regime also appears when the rate of production Φ_a of the available potential energy is compared with the rate of destruction $\Phi_d - \Phi_i$ (Fig. 4). Both

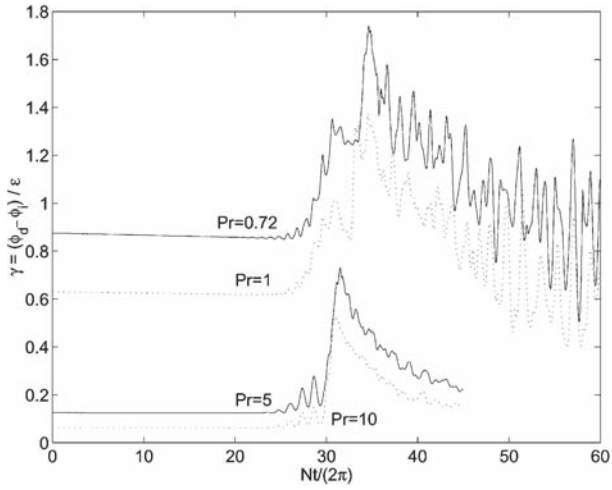


Fig. 3. Mixing efficiency defined by Eq. (7) as a function of time (scaled by the Brunt–Väisälä period) for the same runs as in Fig. 2. The $Pr = 1$ run is also shown for comparison.

advective and diffusive fluxes coincide during the initial stable regime but strongly depart when breaking starts: Φ_a displays alternately positive and negative values while $\Phi_d - \Phi_i$ remains positive and filters out, in a sense, the oscillations displayed by Φ_a . Once breaking has occurred (for $Nt/2\pi > 45$), the fluctuating diapycnal flux relaxes toward zero and may be interpreted as the temporal average of Φ_a .

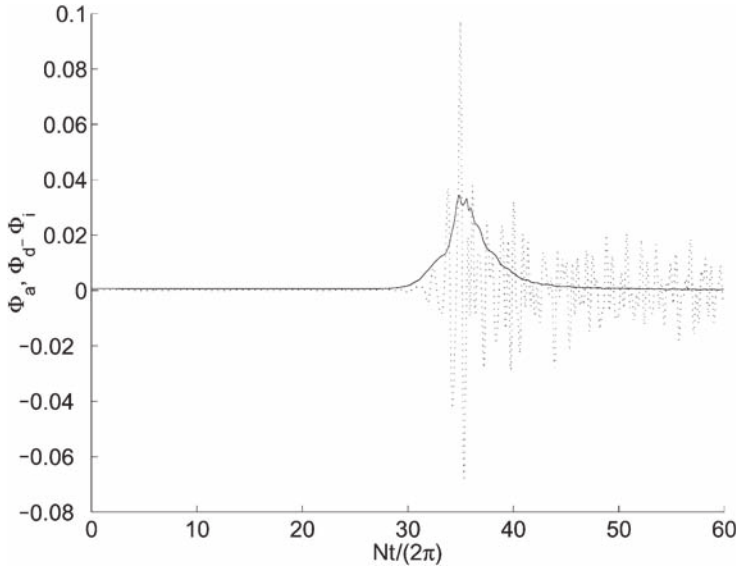


Fig. 4. Vertical advective flux of density Φ_a and fluctuating diapycnal flux $\Phi_d - \Phi_i$ vs. time for the $Pr = 0.72$ run. Time is scaled by the Brunt–Väisälä period.

We finally comment upon the initial behavior of γ displayed in Fig. 3: γ has a constant value, which is Prandtl number dependent. This is consistent with the fact that, for a low amplitude internal gravity wave propagating in a linearly inviscid stratified fluid in an infinite domain, γ is equal to $1/Pr$; the sorted density profile and the linear density profile coincide at any time in this case because the flow is inviscid. Fig. 3 shows that the constant initial values of γ actually underestimate by 37% the theoretical prediction $1/Pr$. The reason is that the sorted density profile does not coincide with the linear density profile near the horizontal boundaries of the fluid domain. A strong density gradient is observed instead at the horizontal boundaries, which modifies Φ_d and, consequently, γ . The steepening of the density gradient near the boundaries is caused by the application of the sorting process in a bounded domain with periodic boundary conditions: at the lower boundary for instance, positive density fluctuations correspond to particles which would have been displaced upward in a infinite domain, thus stemming from a lower altitude, where the fluid is denser. The influence of this effect weakens when breaking occurs because strong gradients are created in the fluid interior as well.

4. Stably stratified homogeneous turbulence

4.1. Overall flow dynamics

Stably stratified homogeneous turbulence with a uniform density (or temperature) profile has been studied by many authors in the past, using laboratory and numerical experiments. In the latter case, a stably stratified turbulent flow is created by a method that has become standard (Riley et al., 1981): a velocity field is initialized in spectral (Fourier) space through a prescribed kinetic energy spectrum (usually peaked about a given wavenumber that sets the scale at which energy is injected) and evolves temporally up to the time t_0 the triple correlations have built. (In practice, this time is estimated by the skewness factor to have reached a value of order 0.45 or so, according to laboratory experiments, implying that a fully turbulent flow has developed.) The velocity field at $t = t_0$ is used as the initial condition of a stably stratified flow, created by setting the Brunt–Väisälä frequency to a non-zero value at $t = t_0$. A density field may also be imposed at this time. In the simulations we present below, this density field is set so that it has the same spectral distribution as the velocity field at $t = t_0$ and the potential energy is half the kinetic energy of the flow at $t = t_0$.

We solve the three-dimensional Boussinesq equations in a cubic numerical domain with periodic boundary conditions. These equations are

$$\frac{\partial \vec{u}}{\partial t} + (\vec{u} \cdot \nabla) \vec{u} = -\frac{1}{\rho_0} \nabla P - \rho' \vec{i}_z + \nu \nabla^2 \vec{u}, \quad (16)$$

$$\frac{\partial \rho'}{\partial t} + (\vec{u} \cdot \nabla) \rho' = N^2 w + \frac{\nu}{Pr} \nabla^2 \rho', \quad (17)$$

$$\nabla \cdot \vec{u} = 0. \quad (18)$$

The notations are the same as in the previous section: $\vec{u} = (u, v, w)$ is the velocity field, P denotes the pressure field and $\rho'(x, y, z, t)$ refers to the field of density fluctuations about

a hydrostatic balanced state, scaled like an acceleration. ν and Pr , respectively, denote the kinematic viscosity and the Prandtl number of the fluid (defined by (11)). The numerical method has been described in Section 2.2.

A number of runs initialized by the method described above has been performed, at resolution 256^3 , in which N is equal to π or $\pi/2$ and $1/\nu$ is varied from 150 to 400, the Prandtl number having the constant value of 1. Two runs will be presented in this section, corresponding to $N = \pi/2$ and $N = \pi$, the viscosity having the value $1/300$ in both cases. The dynamics of these flows is best described in terms of three dimensional parameters, namely a Froude number Fr , a Reynolds number Re_λ based upon the Taylor microscale λ and the Prandtl number Pr . In laboratory experiments (e.g. Lienhard and Van Atta, 1990; Yoon and Warhaft, 1990), the Froude number is commonly defined by the ratio of two length scales, a buoyancy length scale $L_\rho = w'/N$, which is the greatest distance a fluid particle can move against the density gradient and an integral length scale $L = u'^3/\epsilon$, which characterizes the scale of the largest energetic structures. u' and w' denote the *rms* value of the u and w velocity components, respectively. Thus

$$Fr = \frac{L_\rho}{L} = \frac{\epsilon}{N} \frac{w'}{u'^3}, \quad Re_\lambda = \frac{u'\lambda}{\nu}. \quad (19)$$

As is well-known, the buoyancy force stabilizes the flow, in converting vertical kinetic energy into potential energy, the latter energy being involved in irreversible processes such as nonlinear transfers toward small scales (at a faster rate than kinetic energy, e.g. Holloway, 1988; Lesieur, 1997; Staquet and Godeferd, 1998) and molecular mixing. Consequently, as time evolves, the flow organizes into quasi-horizontal layers (e.g. Metais and Herring, 1989). This organization of the flow leads to a strong variability of the velocity components along the vertical direction, which is best put forward by considering the vertical derivative of a velocity component. An iso-surface of $\partial v/\partial z$ is thus displayed in Fig. 5 (see caption) at the end

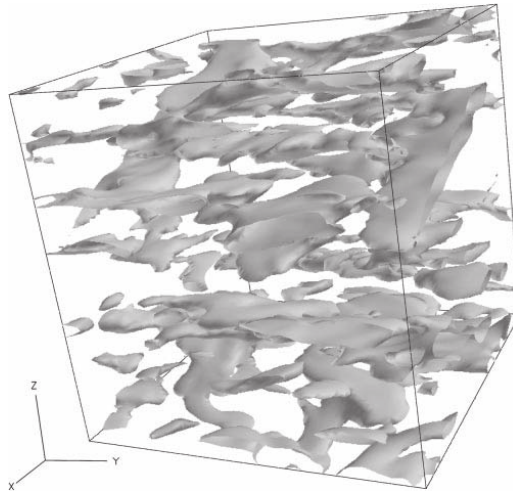


Fig. 5. Run with $N = \pi$ at 6 Brunt–Väisälä periods. Iso-surface of $\partial v/\partial z$ of value equal to 25% of the maximum value of $\partial v/\partial z$ in the fluid domain at that time (from Godeferd and Staquet, 2001).

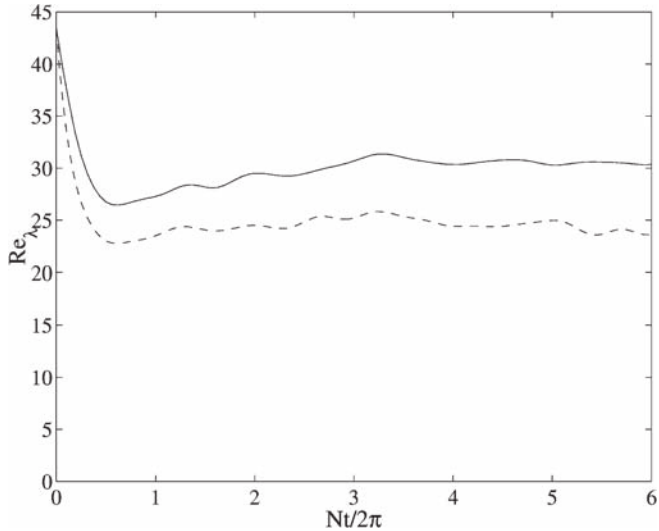


Fig. 6. Temporal evolution of the Reynolds number based upon the Taylor microscale, defined by (19) for the two following runs, (—): $\nu = 1/300$, $N = \pi$; (---): $\nu = 1/300$, $N = \pi/2$. Time is scaled by the Brunt–Väisälä period $2\pi/N$.

of the simulation with $N = \pi$. Since more energy is left in the horizontal plane, a horizontal velocity component is considered. This horizontal velocity component may be arbitrarily chosen because the flow is statistically isotropic about the vertical direction (so that $u \simeq v$).

The temporal evolution of Re_λ is displayed in Fig. 6 for the two runs discussed in this section. Re_λ starts from a value close to 45 and, from $Nt/2\pi \simeq 3$, relaxes toward a nearly constant value. This value depends upon N , which shows that the evolution of Re_λ is not solely driven by buoyancy effects; the reason is that u' is mostly contributed by (large scale) horizontal motions. We found that other quantities relax toward a constant value from this time on, such as the ratio u'/w' (Godeferd and Staquet, 2001). This ratio remains close to the value of 1.4 from about $Nt/2\pi \simeq 2$, in good agreement with laboratory experiments (Lienhard and Van Atta, 1990; Yoon and Warhaft, 1990). This suggests that a weakly turbulent, and even quasi-balanced, dynamical state may have been reached.

4.2. Analysis of mixing

As discussed in the previous section, the sorted density profile is close at all times to the linear density profile in such a homogeneous flow so that the available potential energy E_a may be approximated by the variance of the density fluctuations about either profile: $E_a \simeq 0.5\langle\rho'^2\rangle/N^2$, where $\langle\cdot\rangle$ denotes a volume average (the validity of this approximation is discussed in Holliday and McIntyre, 1981). It follows that a simple expression for the fluctuating diapycnal flux $\Phi_d - \Phi_i$ is provided by the dissipation rate of the fluctuating density variance $\chi = \kappa\langle|\nabla\rho'|^2\rangle$ divided by N^2 : $\Phi_d - \Phi_i \simeq \chi/N^2$. This estimate is commonly used in the ocean (see, e.g. Toole, 1998 for a review). In this context, the mixing efficiency γ should be defined by $\gamma_h = \chi/(N^2\epsilon)$, the volume averaged diapycnal

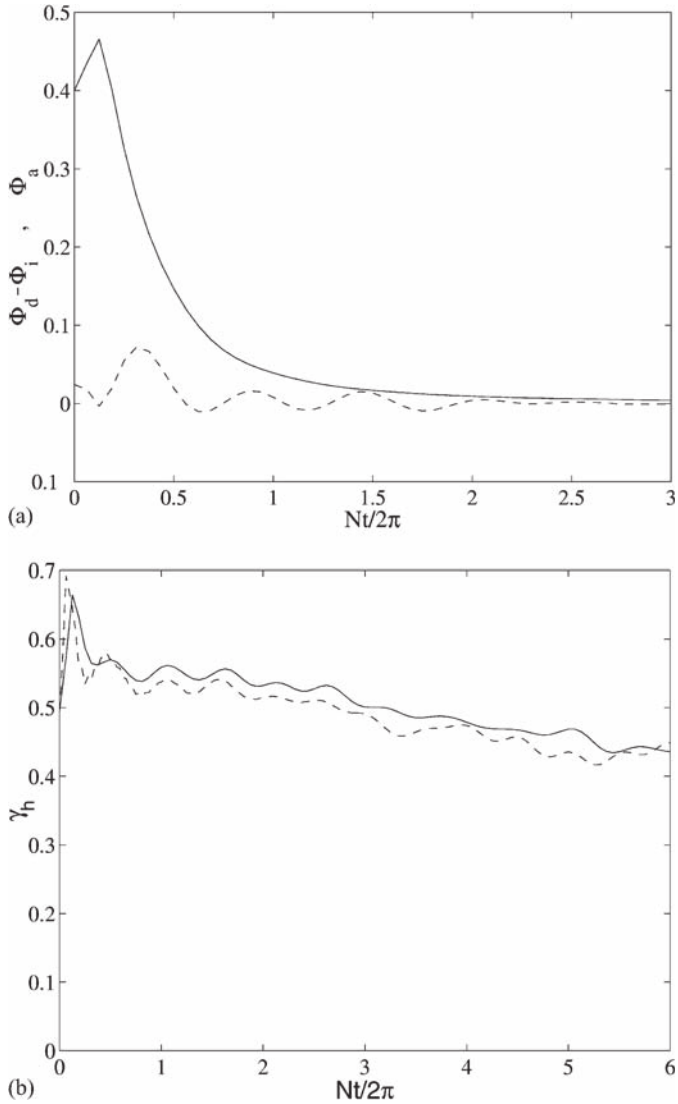


Fig. 7. (a) Comparison of the fluctuating diapycnal flux $\Phi_d - \Phi_i$ (—) with the advective flux of density Φ_a (---) for the $N = \pi$ run. (b) Temporal evolution of the mixing efficiency γ_h , defined in Section 4.2, (—): $N = \pi$; (---): $N = \pi/2$. Time is scaled by the Brunt-Väisälä period $2\pi/N$.

diffusivity by $K_h = \chi/N^4$ and the Cox number by $Co_{x_h} = \chi/(\kappa N^4)$. The index h stands for homogeneous.

Fig. 7a displays the rate of production Φ_a and the rate of destruction $\Phi_d - \Phi_i$ of the available potential energy. Both quantities nearly coincide during the final regime of the flow which attests that a quasi-steady regime has been reached.

The temporal evolution of γ_h is plotted in Fig. 7b for the two runs we consider. As opposed to Re_λ , the curves nearly coincide which shows that the evolution of γ_h is driven by the

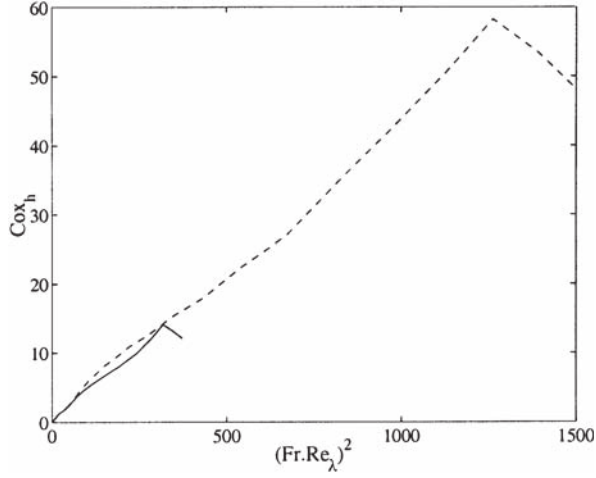


Fig. 8. Cox number $Cox_h(t)$ as a function of $(Fr(t)Re_\lambda(t))^2$, where Fr denotes a Froude number and Re_λ , a Reynolds number based upon the Taylor microscale, for all times of the two runs described in Fig. 6. (---): $N = \pi/2$; (—): $N = \pi$. All parameters are defined in Section 4.

accumulated effect of buoyancy. Apart from the very initial stage of the computation where a 0.7 value is reached, γ_h remains close to 0.45 at all times while slowly decaying.

In order to relate the mixing properties of the flow to the large scale dynamics, we express the Cox number Cox_h as a function of the Froude number Fr defined by Eq. (19). When a dependency as a function of Fr^2 is sought, a simple expression is obtained

$$Cox_h = \frac{Pr}{20} \left(\frac{u'}{w'} \right)^2 \gamma_h (Fr Re_\lambda)^2. \quad (20)$$

This expression involves Re_λ and u'/w' , in addition to γ_h (we recall that $Pr = 1$). The former three quantities relax toward a constant value as time elapses, implying that the Cox number should behave linearly upon Fr^2 when Fr is small enough. This is attested in Fig. 8, where Cox_h is plotted as a function of $(Fr Re_\lambda)^2$ for the runs we consider. The slope of the linear dependency is about 0.045, in good agreement with the large time value of its theoretical expression (taking $Pr = 1$, $\gamma_h = 0.45$ and $u'/w' = 1.4$ yields $Pr/20(u'/w')^2\gamma_h = 0.044$). One interest of this linear dependency is that, conversely, it provides an estimate of the mixing efficiency if the other parameters are known.

5. Stably stratified shear layer in two and three dimensions

5.1. Overall flow dynamics

The shear layer is the simplest case of an inhomogeneous flow. It is formed by two layers of fluids having different densities and horizontal velocities. The interface between

the layers, which thickens by molecular diffusion, enlarges most efficiently if the interface is unstable. A necessary condition for instability is the Richardson number

$$J = \min_z \frac{g}{\rho_0} \frac{-d\bar{\rho}/dz}{(d\bar{U}/dz)^2} \quad (21)$$

to have a value smaller than 0.25 somewhere in the fluid (see, e.g. Drazin and Read, 1981). The overbar in Eq. (21) refers to a horizontal average. If this condition is met, the Kelvin–Helmholtz instability may develop in the vertical plane of the unstable shear flow. It is therefore a two-dimensional instability. As its amplitude grows, nonlinear effects gain importance and makes it saturate while the flow vorticity organises into quasi-horizontal billows. The billows are most unstable to a (two-dimensional) subharmonic instability which makes them pair (see, e.g. Ho and Huerre, 1984 for a review). Secondary three-dimensional instabilities may also occur, at smaller scales than the two-dimensional instabilities. Further detail about the three-dimensional instabilities in a stably stratified shear layer may be found in, e.g. Schowalter et al. (1994), Klaassen and Peltier (1991) or Caulfield and Peltier (1994).

To investigate the shear layer dynamics and resulting mixing properties, we solve the Boussinesq equations in two and three dimensions. Non-dimensional variables are used: we take half the thickness of the initial velocity profile as a length scale, which we denote as δ_i , half the velocity difference across the flow as a velocity scale (U) and half the density difference across the flow times \sqrt{Pr} , as a density scale ($\Delta\rho\sqrt{Pr}/2$). In three dimensions, the resulting non dimensional equations are

$$\frac{\partial \vec{u}}{\partial t} + (\vec{u} \cdot \nabla) \vec{u} = -\nabla P + J\rho + \frac{1}{Re} \nabla^2 \vec{u}, \quad (22)$$

$$\frac{\partial \rho}{\partial t} + (\vec{u} \cdot \nabla) \rho = \frac{1}{Pr Re} \nabla^2 \rho, \quad (23)$$

$$\nabla \vec{u} = 0. \quad (24)$$

As in the previous section, $\vec{u} = (u, v, w)$ denotes the velocity field with u being the streamwise component and w the vertical one; P and ρ , respectively, are the dynamical pressure deviation and density deviation about a hydrostatic balanced state of reference density ρ_0 . J , Re and Pr are the three parameters, set by the scaling mentioned above, upon which the flow dynamics depend. J and Re are expressed as (Pr is defined by Eq. (11))

$$J = \frac{g}{\rho_0} \frac{\Delta\rho\sqrt{Pr}}{2} \frac{\delta_i}{U^2}, \quad Re = \frac{U\delta_i}{\nu}. \quad (25)$$

The initial mean (horizontally averaged) velocity and density fields are of the error function type, the thickness of the density profile being \sqrt{Pr} larger than that of the velocity profile. The velocity field is destabilized by two- and three-dimensional perturbations. The boundary conditions are periodic along the streamwise (x) and spanwise (y) directions and of free slip type along the vertical. The same numerical method as in the previous sections is employed.

We have performed several runs, in two and three dimensions, in which J ranges between 0.04 and 0.16 and Pr has a value of 0.7 or 1.4. The resolution is $(N_x, N_z) = (1024, 1025)$

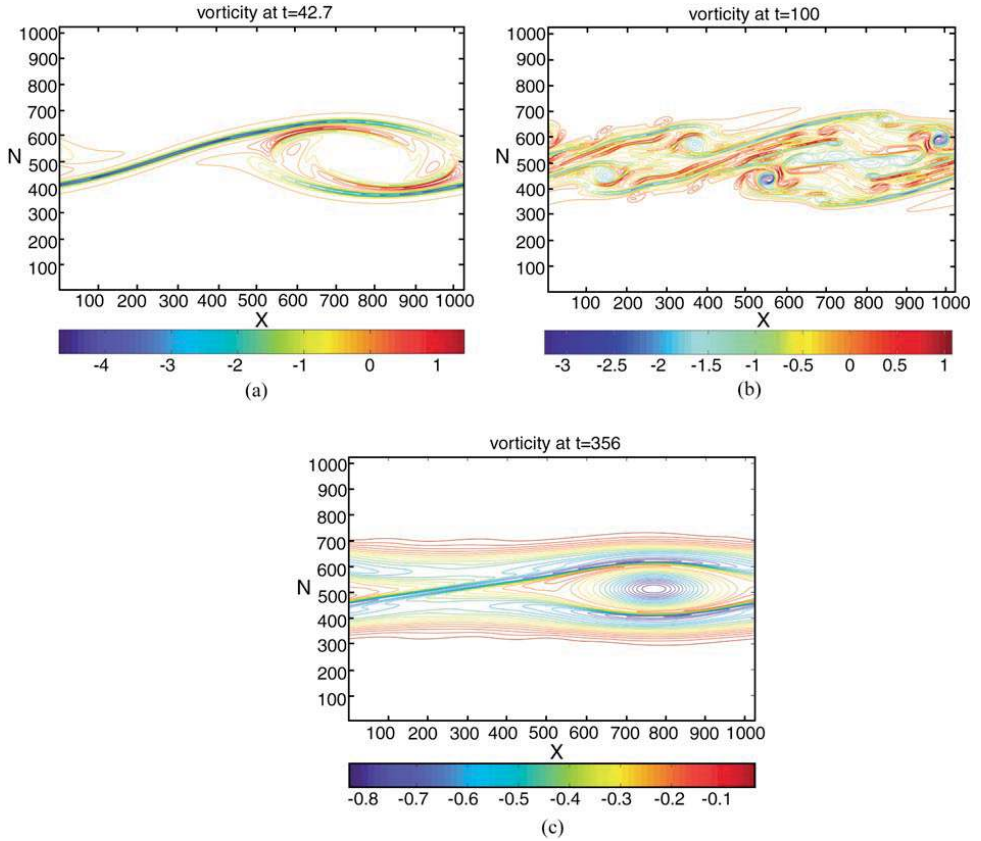


Fig. 9. Vorticity contours of a shear layer evolving in a vertical plane ($J = 0.16$, $Re = 2000$, $Pr = 0.7$). (a) The Kelvin–Helmholtz instability has developed and saturated. (b) Turbulent regime, once two-dimensional *secondary* instabilities have developed. (c) Final time of the simulation: a steady regime (apart from diffusive effects) has been reached. The time unit is δ_i/U (δ_i and U are defined in Section 5.1).

in two dimensions implying that a high Reynolds number can be chosen ($Re = 1000$ or 2000); in three dimensions, the resolution is $(N_x, N_y, N_z) = (128, 128, 257)$ and $Re \simeq 300$. (N_i denotes the number of grid points along direction i).

An example of the flow development in two and three dimensions is displayed in Figs. 9 and 10, respectively.

5.2. Analysis of mixing

The mixing properties of a stably stratified shear layer have been studied by a few authors (Koop and Browand, 1979; Scinocca, 1995; Cortesi et al., 1999; Staquet and Winters, 1997; Staquet, 2000; Caulfield and Peltier, 2000). Only in the three latter papers is the method derived by Winters et al. (1995) used.

In such a vertically inhomogeneous flow, the sorted density profile strongly differs from the mean (horizontally averaged) density profile because the vertical scale of the instability is comparable to that of the vertical density gradient (Staquet, 2000). Hence, as opposed to

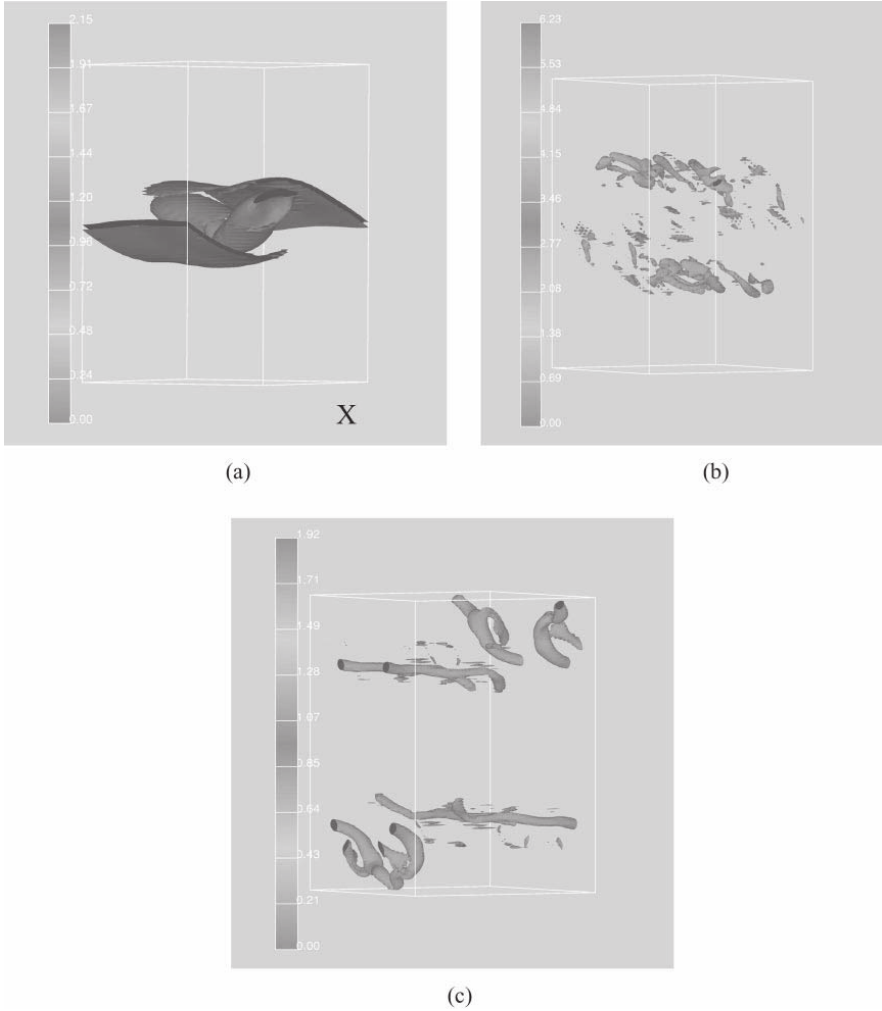


Fig. 10. Temporal evolution of a three-dimensional shear layer simulation with $J = 0.167$, $Re \simeq 300$ and $Pr = 1.4$. A surface equal to $0.5 \max_D(|\omega_x| + |\omega_y| + |\omega_z|)$, where $|\omega_i|$ is the i -component of the vorticity and D the fluid domain, is shown at successive times: (a) $t = 34$, once the Kelvin–Helmholtz instability has grown; the Kelvin–Helmholtz billow, already distorted by the growth of the three-dimensional perturbation, is visible in between vortex sheets (these are the usual braids, reinforced by the baroclinic torque); the streamwise axis is indicated by an X. (b) $t = 108$, when three-dimensional small scale secondary instabilities have developed. (c) $t = 227$, at the end of simulation; only $3/4$ of the numerical domain along the vertical direction is shown for clarity. Time unit is defined in Fig. 9 (from Staquet, 2000).

the previous sections, quantitative information into the mixing properties of the flow can only be gained by using the exact expression of the diapycnal flux, which relies upon the sorted density profile. The mixing efficiency γ defined by Eq. (7) is plotted in Fig. 11a for two-dimensional simulations and in Fig. 11b for three-dimensional simulations. The curves display similar features during the development of the Kelvin–Helmholtz instability (for $t \leq 45$) and during the later stage of the flow (for t larger than $\simeq 150$). By contrast,

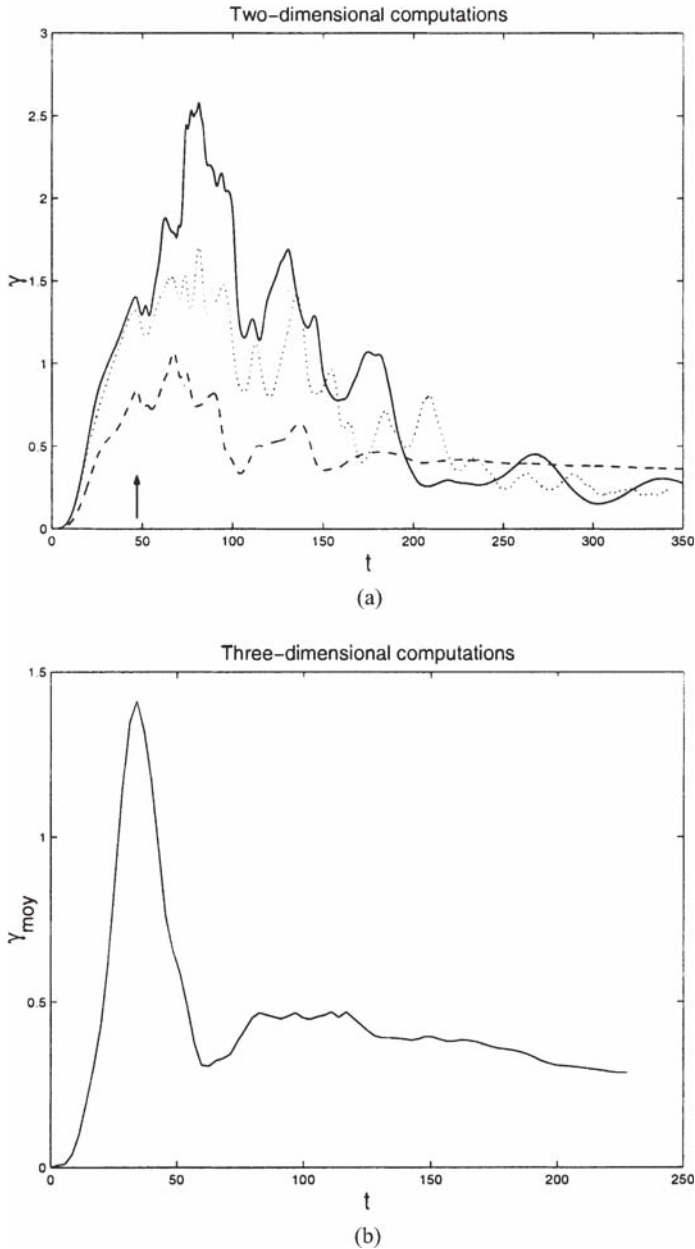


Fig. 11. Mixing efficiency for a stably-stratified shear layer. (a) Two-dimensional shear layer: (—) $Re = 2000$, $Pr = 0.5$, (---) $Re = 1000$, $Pr = 1.4$, (\cdots) $Re = 1000$, $Pr = 0.7$ ($J = 0.167$ for the three computations); the arrow indicates the time at which the Kelvin–Helmholtz instability saturates. (b) Three-dimensional shear layer; the mixing efficiency has been averaged over 7 computations with $0.04 \leq J \leq 0.167$, $Pr = 0.7$ or 1.4 and $Re \simeq 300$. Time unit is defined in Fig. 9.

during the intermediate turbulent regime, the two-dimensional simulations are unable to reproduce the mixing efficiency predicted the three-dimensional simulations because the conservation of enstrophy by nonlinear terms in two dimensions prevents kinetic energy from being efficiently transferred toward small scales. As a consequence, the dissipation rate of kinetic energy has a value too low relative to its three-dimensional counterpart, which overestimates γ .

As in the previous sections, we investigate the relation between the diapycnal diffusivity K_ρ (normalized by the molecular diffusivity κ) and a large scale dynamical parameter. Note that, in the present inhomogeneous flow, the z -dependency of the parameters should be considered (for instance, a volume averaged Cox number would be meaningless). The presence of a mean shear implies that a Richardson number should be taken for the dynamical parameter. We make use of the monotonicity of the sorted density profile ρ_b to introduce a Richardson number that remains one-signed at any time

$$Ri_b(z) = -J \frac{d\rho_b/dz}{(d\bar{U}/dz)^2}. \quad (26)$$

$K_\rho(z)/\kappa$ is plotted as a function of $1/Ri_b(z)$ in Fig. 12 during the final regime of the two-dimensional runs displayed in Fig. 11a, when γ has reached a constant value. A linear dependency is found. It may be expressed by the same simple relation as in the previous sections, though a local formulation should be used to account for the vertical inhomogeneity. Since we deal with a sorted density profile, *local* means here that a given isopycnal is considered. We get

$$\frac{K_\rho(z)}{\kappa} = Pr \frac{\gamma_{loc}(z)}{Ri_b(z)} + 1 \quad (27)$$

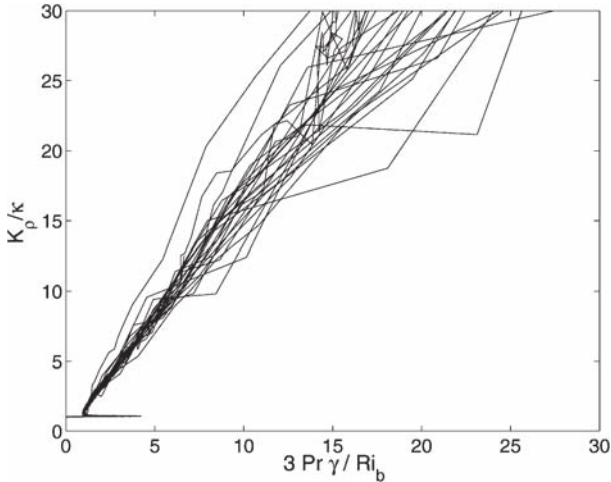


Fig. 12. Diapycnal diffusivity $K_\rho(z)$ defined by Eq. (6) as a function of the inverse of the Richardson number $Ri_b(z)$ defined by Eq. (26). The different curves correspond to successive times of the final regime of a two-dimensional simulation with $J = 0.167$, $Re = 1000$, $Pr = 1.4$.

where $\gamma_{\text{loc}}(z) = (\phi_{\text{d}}(z) - \phi_{\text{i}}(z))/\epsilon_{\text{loc}}(z)$ is a local mixing efficiency ($\phi_{\text{i}}(z) = -\kappa \text{d}\rho_{\text{b}}/\text{d}z$), which depends upon z a priori; we have also assumed that the local (in the above sense) dissipation rate of kinetic energy is mostly contributed by the vertical shear of the mean flow: $\epsilon_{\text{loc}}(z) \simeq 2\nu(\text{d}\bar{U}/\text{d}z)^2$.

The linear dependency we find in Fig. 12 implies that γ_{loc} is actually a constant function of z . We found that this constant function has a value equal to 3γ . When the same analysis is conducted in a three-dimensional shear layer, this linear dependency is not recovered, even when $Ri_{\text{b}}(z)$ is defined using either a sorted or a horizontally averaged dissipation rate divided by 2ν (instead of $(\text{d}\bar{U}/\text{d}z)^2$). Hence, in general, γ_{loc} is a non trivial function of z .

The finding of a constant value in the two-dimensional shear layer but not in the three-dimensional one suggests to analysing the main differences between the two- and three-dimensional flow dynamics during the final regime. One important difference is that a quasi-steady state has been reached in two dimensions. For instance, the advective flux Φ_{a} nearly matches the fluctuating diapycnal flux $\Phi_{\text{d}} - \Phi_{\text{i}}$ during this later stage (Staquet, 2000). The same result holds for the final regime of breaking gravity waves (Fig. 4) as well as of homogeneous stably stratified turbulence (Fig. 7a). The second difference is that the flow has organized into layers during this final regime, which implies that the dissipation rate of kinetic energy is mainly contributed by the vertical variability of horizontal motions. In homogeneous stably stratified turbulence for instance, 60% of ϵ is contributed by $\nu(\partial u/\partial z)^2$ (Godeferd and Staquet, 2001) and we found this ratio to be higher for low amplitude breaking gravity waves. This is also the case in the two-dimensional shear layer but does not hold at all during the final stage of the three-dimensional shear layer.

6. Conclusion

We have studied the mixing properties of three stably stratified flows: breaking gravity waves, a homogeneous stably stratified decaying turbulence and a stably stratified shear layer in two and three dimensions. We have found that, during the final regime of the homogeneous flows (stably stratified turbulence and breaking gravity waves) and of the two-dimensional stably stratified shear layer, the diapycnal diffusivity behaves linearly as a function of a Froude number squared when the flow is homogeneous and as a function of the inverse of a Richardson number in the two-dimensional shear layer case. This behaviour can be accounted for by a simple expression which shows that the coefficient of the linear law is the mixing efficiency of the flow, γ , times the Prandtl number of the fluid. Such a linear law thus amounts to the scaling often assumed by oceanographers (e.g. Munk and Wunsch, 1998). The mixing efficiency is volume averaged in the homogeneous case and averaged over an isopycnal in the shear layer case. This linear law implies that γ has reached a constant value.

When analysing the final regime of the three flows sharing this common linear law, we find that a quasi-steady stable state has been reached, in which the production and dissipation rates of available potential energy balance; also, the dissipation rate of kinetic energy is mostly contributed by the vertical variability of horizontal motions. Thus, the flow has become weakly turbulent and organized into layers. Further work remains to be done to understand whether such a linear law is a generic mixing property of this type of flow.

Acknowledgements

Computations were performed at the Computer Center of CNRS (IDRIS).

References

- Benielli, D., Sommeria, J., 1996. Excitation of internal waves and stratified turbulence by parametric instability. *Dyn. Atmos. Oceans* 23, 335.
- Bouruet-Aubertot, P., Sommeria, J., Staquet, C., 1995. Breaking of internal gravity waves through two-dimensional instabilities. *J. Fluid Mech.* 285, 265–301.
- Bouruet-Aubertot, P., Sommeria, J., Staquet, C., 1996. Stratified turbulence produced by internal wave breaking: two-dimensional numerical experiments. *Dyn. Atmos. Oceans* 23, 357–369.
- Bouruet-Aubertot, P., Koudella, C., Staquet, C., Winters, K.B., 2001. Particle dispersion and mixing by breaking internal gravity waves: two-dimensional numerical experiments. *Dyn. Atmos. Oceans* 33 (2), 95–134.
- Canuto, C., Hussaini, M.Y., Quarteroni, A., Zang, T.A., 1988. *Spectral Methods in Fluid Dynamics*, Springer Series in Computational Physics. Springer, Berlin.
- Caulfield, C.P., Peltier, W.R., 1994. Three-dimensionalization of the stratified mixing layer. *Phys. Fluids* 6 (12), 3803–3805.
- Caulfield, C.P., Peltier, W.R., 2000. The anatomy of the mixing transition in homogeneous and stratified free shear layers. *J. Fluid Mech.* 413, 1–47.
- Cortesi, A.B., Smith, B.L., Yadigaroglu, G., Banerjee, S., 1999. Numerical investigation of the entrainment and mixing processes in neutral and stably stratified shear layers. *Phys. Fluids* 11 (1), 162–185.
- Drazin, P.G., 1977. On the instability of an internal gravity wave. *Proc. R. Soc. London A* 356, 411–432.
- Drazin, P.G., Read, W.H., 1981. *Hydrodynamic Stability*. Cambridge University Press, Cambridge.
- Fernando, H.J.S., 1991. Turbulent mixing in stratified flows. *Ann. Rev. Fluid Mech* 23, 455–493.
- Godeferd, F.S., Staquet, C., 2001. Statistical modelling and direct numerical simulations of decaying stably-stratified turbulence: Part 2. Large and small scale anisotropy. *J. Fluid Mech.*, submitted for publication.
- Hannoun, I.A., List, E.J., 1988. Turbulent mixing at a shear-free density interface. *J. Fluid Mech.* 189, 211–234.
- Ho, C.M., Huerre, P., 1984. Perturbed free shear layers. *Ann. Rev. Fluid Mech.* 16, 365–424.
- Holliday, D., McIntyre, M.E., 1981. On potential energy density in an incompressible stratified fluid. *J. Fluid Mech.* 107, 221–225.
- Holloway, G., 1988. The buoyancy flux from internal gravity wave breaking. *Dyn. Atmos. Oceans* 12, 107.
- Imberger, J., Boashash, B., 1986. Application of the Wigner-Ville distribution to temperature gradient microstructure: a new technique to study small-scale variations. *J. Phys. Oceanogr.* 16, 1997–2012.
- Klaassen, G.P., Peltier, W.R., 1991. The influence of stratification on secondary instability in free shear layers. *J. Fluid Mech.* 227, 71–106.
- Klostermeyer, J., 1991. Two and three-dimensional parametric instabilities in finite amplitude internal gravity waves. *Geophys. Astrophys. Fluid Dyn.* 61, 1–25.
- Koop, C.G., Browand, F.K., 1979. Instability and turbulence in a stratified fluid with shear. *J. Fluid Mech.* 93, 135–159.
- Koudella, C.R., 1999. Ondes internes de gravité en fluide stratifié: instabilités, turbulence et vorticité potentielle. Thèse de l'École Normale Supérieure de Lyon.
- Koudella, C.R., Staquet, C., 2001. Two-dimensional instability mechanisms of a progressive internal gravity wave. *Phys. Fluids*, in preparation.
- Lesieur, M., 1997. *Turbulence in Fluids*, 3rd Edition. Kluwer Academic Publishers, Dordrecht.
- Lienhard, J.H., Van Atta, C.W., 1990. The decay of turbulence in thermally stratified flow. *J. Fluid Mech.* 210, 57–112.
- Lombard, P.N., Stretch, D.D., Riley, J.J., 1990. Energetics of a stably stratified mixing layer. In: *Proceedings of the Ninth Symposium on Turbulence and Diffusion*. AMS, Cleveland, OH, pp. 202–206.
- Lorenz, E.N., 1955. Available potential energy and the maintenance of the general circulation. *Tellus* 7, 157–167.
- McEwan, A.D., 1983. Internal mixing in stratified fluids. *J. Fluid Mech.* 128, 59–80.

- Mied, R.P., 1976. The occurrence of parametric instabilities in finite amplitude internal gravity waves. *J. Fluid Mech.* 78, 763–784.
- Métais, O., Herring, J.R., 1989. Numerical simulations of freely evolving turbulence in stably stratified fluids. *J. Fluid Mech.* 202, 117–148.
- Munk, W., Wunsch, C., 1998. Abyssal recipes II: energetics of tidal mixing and wind mixing. *Deep Sea Research* I 45, 1977–2010.
- Orszag, S.A., 1971. Numerical simulation of incompressible flows within simple boundaries. I. Galerkin (spectral) representation. *Stud. Appl. Maths.* 50 (4), 293–327.
- Osborn, T.R., Cox, C.S., 1972. Oceanic fine structure. *Geophys. Fluid Dyn.* 3, 321–345.
- Riley, J.J., Metcalfe, R.W., Weissman, M.A., 1981. Direct numerical simulations of homogeneous turbulence in density-stratified fluids. in: West, B.J. (Ed.), *Proceedings of AIP Conference on Nonlinear Properties of Internal Waves*, American Institute of Physics, New York, pp. 79–112.
- Schowalter, D.G., Lasheras, J.C., van Atta, C.W., 1994. A study of streamwise vortex structure in a stratified shear layer. *J. Fluid Mech.* 281, 247–291.
- Scinocca, J.F., 1995. The mixing of mass and momentum by Kelvin–Helmholtz billows. *J. Atmos. Sci.* 52 (14), 2509–2530.
- Staquet, C., 2000. Mixing in a stably stratified shear layer: two- and three-dimensional numerical experiments. *Fluid Dyn. Res.* 27, 367–404.
- Staquet, C., Godeferd, F.S., 1998. Statistical modelling and direct numerical simulations of decaying stably-stratified turbulence: I. Flow Energetics. *J. Fluid Mech.* 360, 295–340.
- Staquet, C., Winters, K.B., 1997. Mixing in a stably-stratified shear layer. In: Binder, G. (Ed.), *Proceedings of the XIth Symposium on Turbulent Shear Flows*, Vol. 2, Session 20, pp. 25–30.
- Taylor, J.R., 1992. The energetics of breaking events in a resonantly forced internal wave field. *J. Fluid Mech.* 239, 309–340.
- Toole, J., 1998. Turbulent mixing in the ocean: intensity, causes and consequences. In: Chassignet, E., Verron, J. (Eds.), *Proceedings of Les Houches Winter School*, January 1998.
- Thorpe, S.A., 1977. Turbulence and mixing in a Scottish Loch. *Phil. Trans. R. Soc. London A* 286, 125–181.
- Winters, K.B., Lombard, P.N., Riley, J.J., D’Asaro, E.A., 1995. Available potential energy and mixing in density-stratified fluids. *J. Fluid Mech.* 289, 115–128.
- Winters, K.B., D’Asaro, E.A., 1996. Diascalar flux and the rate of fluid mixing. *J. Fluid Mech.* 317, 179–193.
- Yoon, K., Warhaft, Z., 1990. The evolution of grid-generated turbulence under conditions of stable thermal stratification. *J. Fluid Mech.* 215, 601–638.